Journal of Materials Science: Materials in Engineering

ORIGINAL PAPER

Open Access

Sintering and electrical conductivity of calcium-doped three-cation perovskite materials

Sai Ram Gajjala[1], Geoffrey A. Swift[1*] and Rasit Koc[1]

Abstract

$La_{1-x}Ca_x(B1,B2,B3)O_3$ perovskite powders doped with calcium were synthesized and sintered. Calcium doping modified the A-site of the perovskite structure, while the B-site was composed of three cations in equal atomic amounts. Cations on the B-site included cobalt, chromium, iron, manganese, and nickel. Sintering temperature varied from 1200 to 1400 °C in air. Density measurements and microstructure imaging determined effect of composition on sintering. Electrical conductivity of sintered compacts was measured using the four-wire measurement method at temperatures of 300 to 900 °C in air. Electrical properties as a function of composition indicate the effect of calcium doping in combination with varied B-site substitution increases electrical conductivity and improves sintering.

Keywords Perovskite, Doping, Sintering, Conductivity, Oxide

Introduction

Calcium-doped lanthanum perovskites

Lanthanum-based perovskites have been developed for use in solid oxide fuel cells (SOFCs) as both interconnect materials and cathode materials. Lanthanum perovskite has the general chemical formula ABO_3, A is the A-site cation, lanthanum in this case, and B is the B-site cation. The B-site cation is often chromium, i.e., $LaCrO_3$. Doping on the A-site and substitution on the B-site can modify the properties of the perovskite material by altering the geometry of the crystal structure and affecting the development of pairing between like atoms of different oxidation state (Koc and Anderson 1992; Liu et al. 2023). Increasing the number of cations substituted into the B-site increases the entropy of the perovskite. For example, the B-site can be substituted with one or more elements to affect the sintering behavior, high-temperature properties, and electrical conductivity. Thus, compositions such as $LaCr_{0.5}Co_{0.5}O_3$ have been developed and studied (Kolisetty et al. 2017).

In a similar manner to B-site substitution, doping on the A-site has been investigated. Such studies are often undertaken as a means to reduce the operational temperature of the material by increasing the electrical conductivity, thereby increasing the efficiency of an SOFC employing these materials. That is, if the SOFC can operate at a lower temperature, the fuel cell can be expected to have a longer service life and consume less energy during operation (Sparlin and Raffaelle 1991; Sehlin et al. 1991).

Calcium doping has been studied for the A-site in La-based perovskites. These studies have found that Ca doping can reduce the sintering temperature of the perovskite and reduce the Seebeck coefficient by suppressing the Verwey mechanism (Sehlin et al. 1991).

The present research is concerned with doping on both the A-site in concert with substitution on the B-site in La-based perovskites. The A-site is lanthanum, doped with 10–30 at% Ca, while the B-site is a trio of cations in equal atomic ratio (one-third each) drawn from the

*Correspondence:
Geoffrey A. Swift
geoffrey.swift@siu.edu
[1] School of Mechanical, Aerospace, and Materials Engineering, Southern Illinois University Carbondale, Carbondale, IL 62901, USA

following elements: chromium, cobalt, iron, manganese, and nickel. This combination of B-site substitution and A-site doping is novel and demonstrates unique properties for La-based perovskites. Powders were prepared with these compositions and characterized with X-ray diffraction (XRD). Powders were compacted and sintered in air at varying temperature from 1200 to 1400 °C. Sintered materials were characterized for densification as a function of composition and sintering temperature, and for electrical conductivity as a function of temperature, to determine the effects of A-site doping in concert with B-site substitution. Prior work on Ca-doped La(Co,Cr)O_3 perovskites led to +2/+4 pairing of the B-site cations, which drove the high-temperature Seebeck coefficient to nearly zero and which in combination with A-site Ca doping partially suppressed the Verwey mechanism (Sehlin et al. 1991). The present materials use three atoms equally substituted on B-sites along with A-site doping to eliminate these issues in novel fashion.

Materials and methods

Sample preparation

$La_{1-x}Ca_x(B1,B2,B3)O_3$ powders were prepared using the polymerizable sol-gel technique method (Pechini 1967; Gajjala et al. 2019), where x ranged from 0 to 0.3. B-site cations included three of the following five metals for each composition: Co, Cr, Fe, Mn, and Ni in equal atomic amounts (i.e., one-third each). Table 1 lists the compositions of the nine prepared materials for this study. Starting materials were Alfa Aesar powders of $La_2(CO_3)_3{\cdot}XH_2O$, $Cr(NO_3)_3{\cdot}9H_2O$, $Fe(NO_3)_3{\cdot}9H_2O$, $N_2NiO_6{\cdot}6H_2O$, $Co(NO_3)_2{\cdot}6H_2O$, $MnCO_3$, and $CaCO_3$. XRD (Rigaku D/Max-B diffractometer with Cu Kα ($\lambda = 1.54056$ Å) radiation) determined that the synthesized powders were single phase.

Table 1 Combinations of cations on the A- and B-sites for synthesized powders. B-site cations were present in equal atomic amounts, e.g., $Cr_{1/3}Fe_{1/3}Ni_{1/3}$ for Powder 1. Calcium doping on the A-site used a range of $x = 0$ to $x = 0.3$

Powder no.	A-site	B1	B2	B3
1	$La_{1-x}Ca_x$	Cr	Fe	Ni
2	$La_{1-x}Ca_x$	Cr	Co	Mn
3	$La_{1-x}Ca_x$	Cr	Mn	Ni
4	$La_{1-x}Ca_x$	Cr	Fe	Mn
5	$La_{1-x}Ca_x$	Cr	Co	Fe
6	$La_{1-x}Ca_x$	Cr	Co	Ni
7	$La_{1-x}Ca_x$	Fe	Mn	Ni
8	$La_{1-x}Ca_x$	Co	Fe	Mn
9	$La_{1-x}Ca_x$	Co	Fe	Ni

The resulting powders were uniaxially compacted in a hydraulic press to a pressure of about 14 MPa to produce green pellets. Green pellets were sintered in air at temperatures of 1200 °C, 1300 °C, or 1400 °C. The sintering time was kept constant at 2 h to eliminate that as a variable.

Sintering characterization

Sintered samples were characterized in terms of microstructure and density to determine the effect of sintering temperature for the powder compositions of this study. Sintered sample surfaces were polished and subsequently thermally etched in air at 1200 °C. Sintered microstructures were studied by SEM (FEI Quanta FEG 450). Density was determined using the Archimedes immersion method.

Electrical conductivity

Electrical conductivity of sintered samples was measured using a four-probe sensing technique and an AC resistance bridge (Linear Research Inc. LR-700). Platinum paste was applied to the ends of rectangular sintered $La_{1-x}Ca_x(B1,B2,B3)O_3$ pellets, which were heated in air to 300–900 °C.

Results and discussion

Synthesized powders (XRD)

Figure 1 shows the XRD spectra for Powder 2, $La_{1-x}Ca_x(Co_{1/3}Cr_{1/3}Mn_{1/3})O_3$ as an example of XRD data. The absence of the starting materials indicates that the conversion to the mixed perovskite (undoped and Ca-doped) was complete. The $x = 0$ spectrum exhibits a minor acromion (indicated by the arrow in Fig. 1) associated with La-based perovskite materials (Liu et al. 2023; Gálvez et al. 2015), which is not present in the other samples. This, along with the slight shift toward higher diffraction angle, indicates a slight change in the perovskite structure through the addition of calcium. Similar plots of XRD data indicated conversion of the other compositions.

Sintering characterization

Figure 2 shows the microstructure for undoped $La_{1-x}Ca_x(Co_{1/3}Cr_{1/3}Mn_{1/3})O_3$, i.e., $x = 0$. For these undoped powders, sintering is affected greatly by B-site substitution. Powder 1 showed poor sintering below 1400 °C, while Powder 2 sintered at all temperatures with visible open pores. Powder 3 showed sintering had occurred, but porosity was very high. Powder 4 appeared fully sintered at 1400 °C but with significant porosity when sintered below that temperature. Powder 5 sintered, but porosity was very high. Powder 6 sintered at 1400 °C but with significant porosity. Powder 7 sintered and at 1400

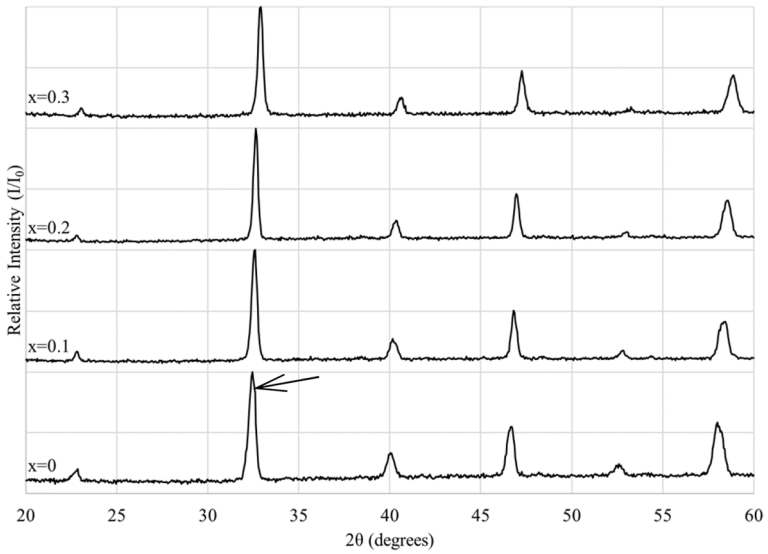

Fig. 1 XRD spectra for $La_{1-x}Ca_x(Co_{1/3}Cr_{1/3}Mn_{1/3})O_3$, for $x = 0$ to 0.3. Conversion of starting materials to single-phase perovskite is indicated by the presence of only perovskite peaks. Arrow indicates an acromion in the $x = 0$ spectrum, which is absent from the other spectra

°C had noticeably reduced porosity compared to lower sintering temperatures. Powder 8 sintered at all temperatures but with less porosity at higher temperatures. Powder 9 showed minimal sintering. Powders 2, 4, and 8 had the best-developed microstructures of the undoped perovskite powders.

Figure 3 shows the microstructure for $La_{1-x}Ca_x(Co_{1/3}Cr_{1/3}Mn_{1/3})O_3$ materials with $x = 0.1$. Calcium doping can be seen to have had an effect on sintering of these B-site substituted powders at this level of doping. Powder 1 now shows a sintered grain structure with minimal porosity at all temperatures. Powder 2, which already showed sintered grains, now lacks the porosity that was present in the undoped powder. Powders 3 and 4 sintered, but large pores remain in the microstructure at 1400 °C. Powder 5 sintered fully at 1400 °C, but below that temperature, significant porosity was present. Powder 6 exhibits a denser microstructure, though some porosity remains. Powder 7 is the lone exception, as it seems to show a lesser degree of sintering at 1400 °C than in the undoped powder. Powders 8 and 9 both have excellent sintered grain structures with no visible porosity after sintering at 1400 °C.

Figure 4 shows the microstructure for $La_{1-x}Ca_x(Co_{1/3}Cr_{1/3}Mn_{1/3})O_3$ materials with $x = 0.2$. This amount of Ca doping at the A-site had several observable effects on the sintered grain structures. Powders 1 through 3 all possessed a fully sintered grain structure at 1400 °C and with smaller grains than for $x = 0.1$. The corners of grains also appeared more rounded. This is indicative of the calcium forming a liquid phase during sintering, which aids densification (Kolisetty et al. 2017). Powder 4 appeared similar to the $x = 0.1$ microstructure, though with larger grains. Powder 5 had sharper, smaller grains than for $x = 0.1$. Powder 6 appears similar but with less porosity than for $x = 0.1$. Powder 7 still had porosity, but the grain size was much smaller, and the microstructure appeared more developed compared to that for $x = 0.1$. Powders 8 and 9 both showed smaller grains with corners that were more rounded than for $x = 0.1$, again indicating the formation of a liquid phase.

Figure 5 shows the microstructure for $La_{1-x}Ca_x(Co_{1/3}Cr_{1/3}Mn_{1/3})O_3$ materials with $x = 0.3$. This maximum amount of Ca doping at the A-site for this research led to several observable effects on the sintered grain structures. Powders 1, 2, 4, 5, 8, and 9 all had rounded grains. The higher amount of Ca led to a greater amount of liquid phase during sintering, as indicated by this grain morphology. Powder 4 still possessed large, closed pores even at 1400 °C. Powders 3, 6, and 7 all exhibited very small grains and reduced porosity compared to other values for x.

Overall, increasing the amount of Ca doping on the A-site for La-based perovskites with three different atom types at the B-site led to superior sintered microstructures, with rounded grains and closed porosity. Because calcium forms a liquid phase when doped onto the A-site, the temperature required for sintering is reduced in several powders, e.g., Powders 1, 2, and 3, which exhibited dense grain structures at 1200 °C for $x = 0.3$.

Table 2 shows the relative density for $La_{1-x}Ca_x$(B1,B2,B3)O_3 materials sintered. For most of the materials under consideration, increasing Ca content on the A-site yielded

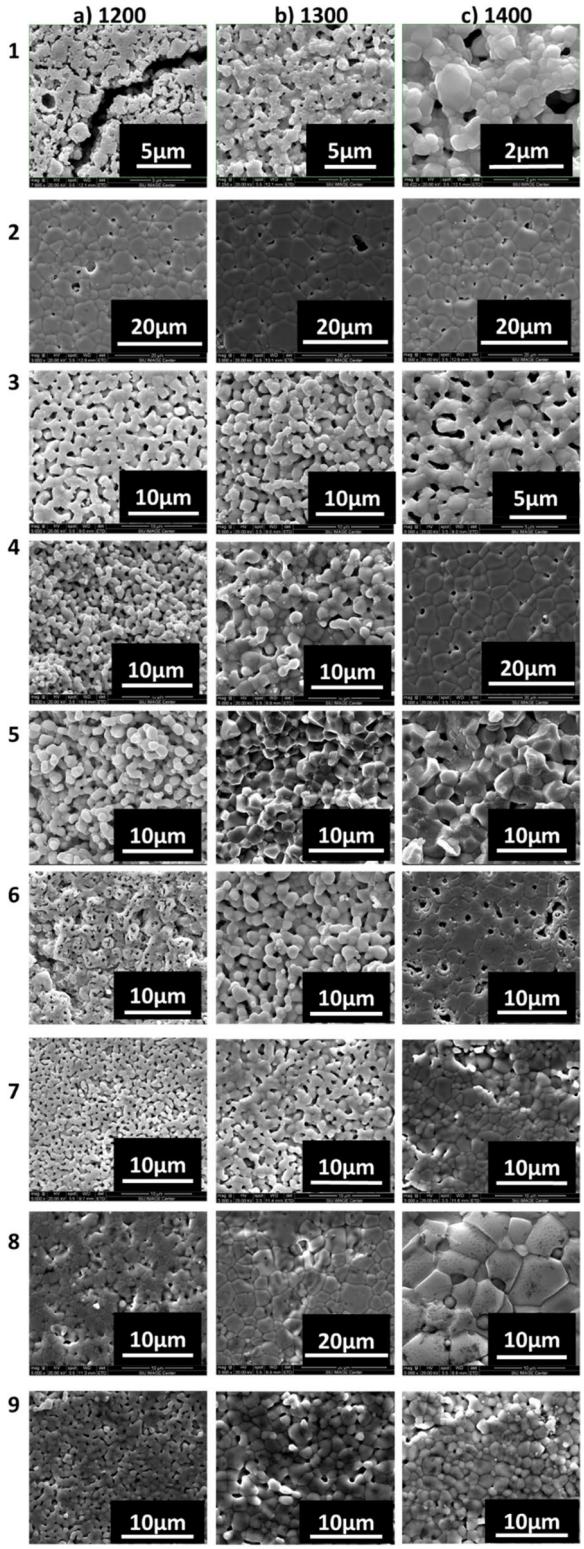

Fig. 2 Microstructures for undoped La perovskite materials sintered at **a** 1200 °C, **b** 1300 °C, and **c** 1400 °C

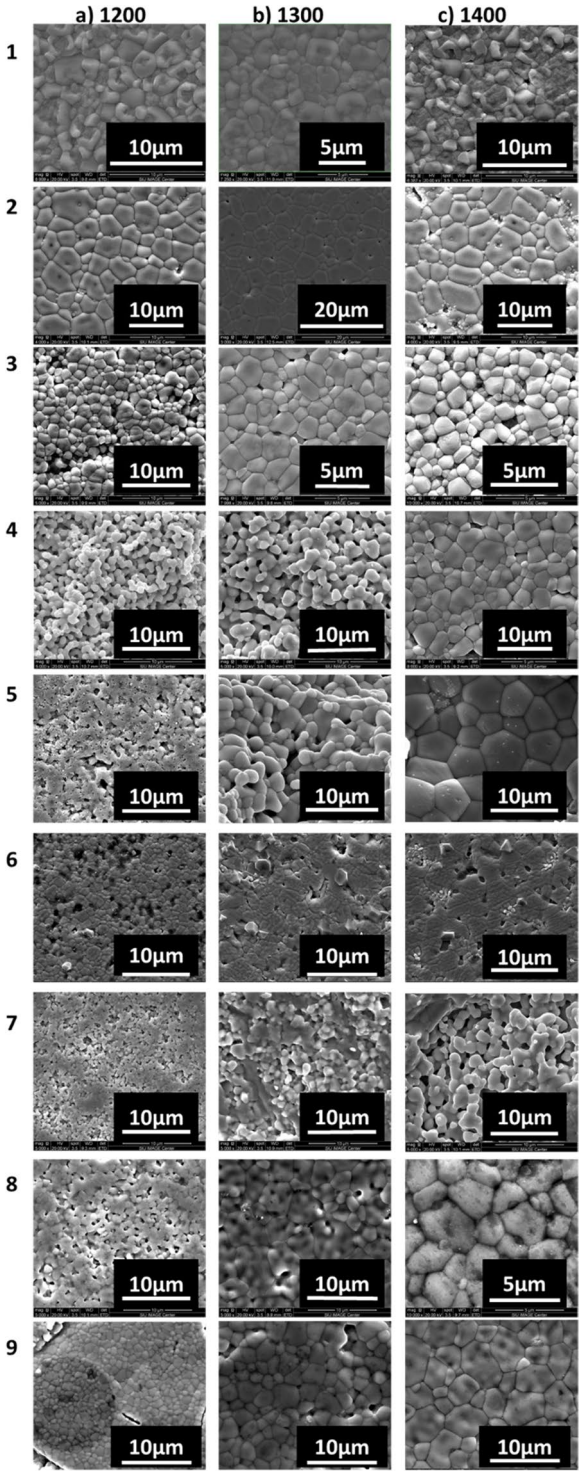

Fig. 3 Microstructures for Ca-doped ($x = 0.1$) La perovskite materials sintered at **a** 1200 °C, **b** 1300 °C, and **c** 1400 °C

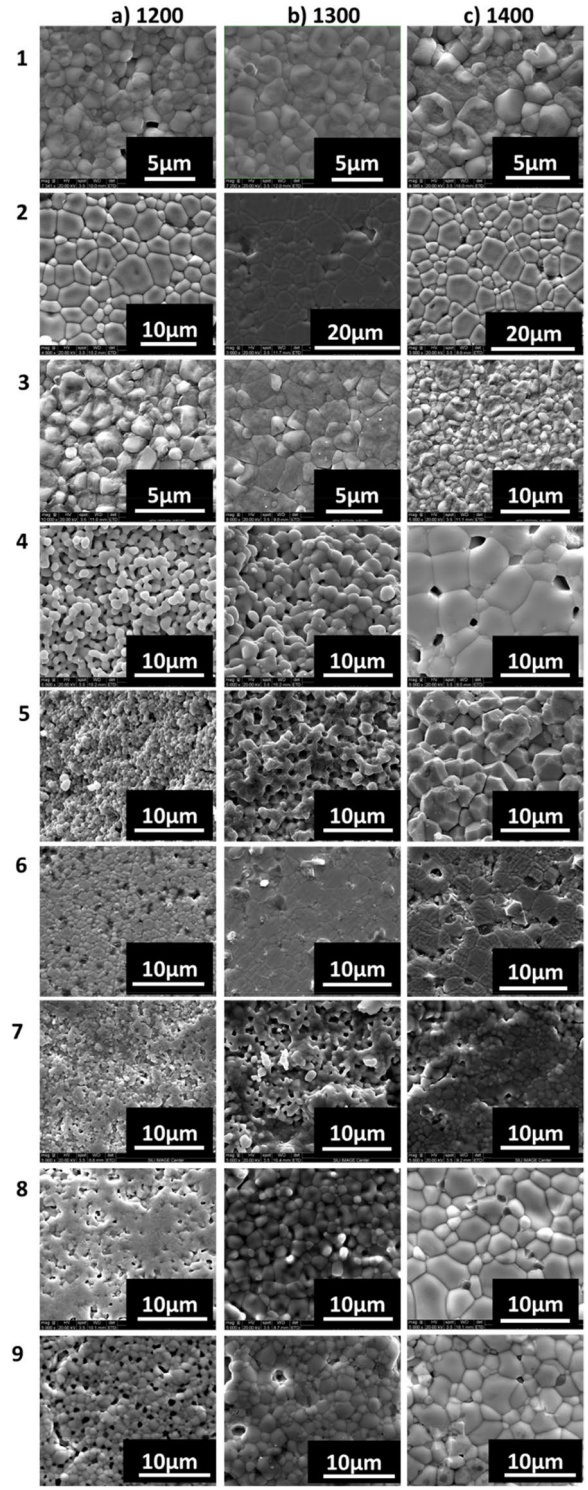

Fig. 4 Microstructures for Ca-doped ($x = 0.2$) La perovskite materials sintered at **a** 1200 °C, **b** 1300 °C, and **c** 1400 °C

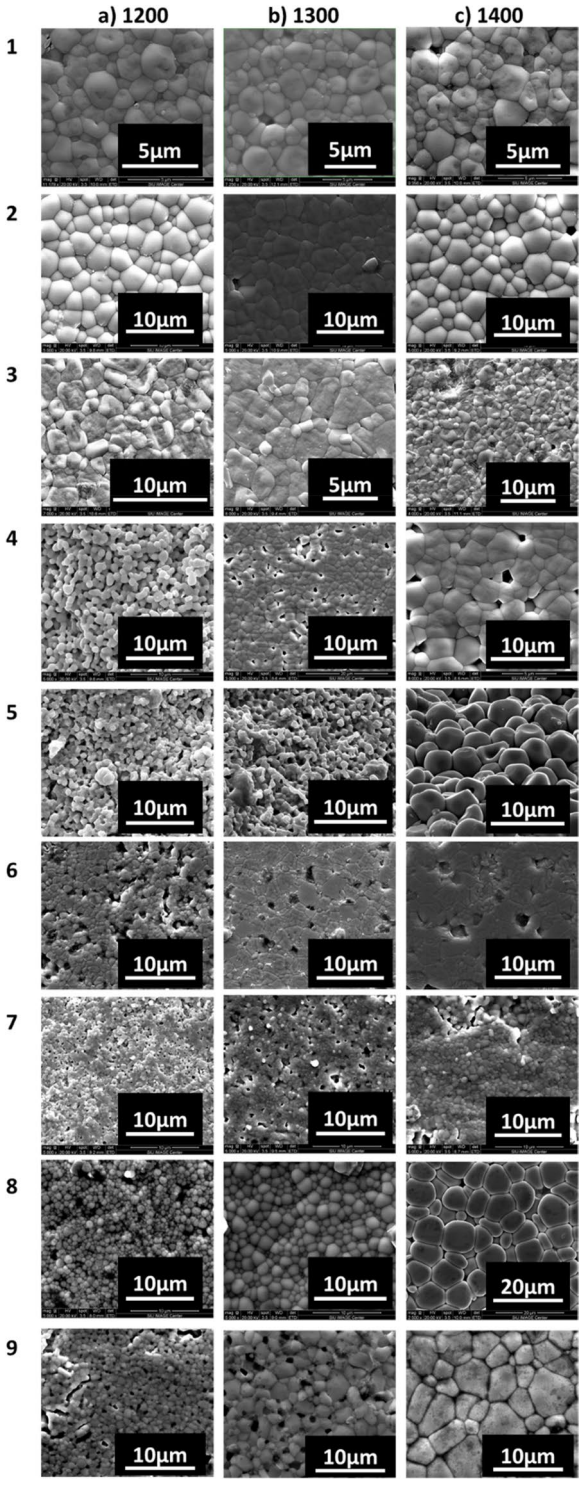

Fig. 5 Microstructures for Ca-doped ($x = 0.3$) La perovskite materials sintered at **a** 1200 °C, **b** 1300 °C, and **c** 1400 °C

Table 2 Relative density (%) for sintered $La_{1-x}Ca_x(B1,B2,B3)O_3$ materials

Powder no.	Temperature (°C)	$x = 0$	$x = 0.1$	$x = 0.2$	$x = 0.3$
1	1200	70	88	94	91
	1300	71	86	90	91
	1400	75	88	91	92
2	1200	73	84	86	82
	1300	78	85	86	90
	1400	84	85	87	90
3	1200	72	78	88	83
	1300	79	86	88	87
	1400	83	83	88	86
4	1200	75	87	98	99
	1300	80	91	99	97
	1400	98	93	96	98
5	1200	90	92	94	94
	1300	91	98	98	97
	1400	97	99	98	95
6	1200	65	69	70	97
	1300	62	69	70	98
	1400	63	67	71	99
7	1200	69	88	92	94
	1300	84	93	99	99
	1400	98	99	99	99
8	1200	91	91	90	96
	1300	97	96	97	98
	1400	98	99	97	93
9	1200	67	77	75	96
	1300	68	68	71	97
	1400	69	72	74	99

a higher relative sintered density. Powder 1, for example, increased from a relative density of 75% with no doping to 92% for doping, where $x = 0.3$ (see Table 2). Powder 7 sintered to a high relative density of 99% for $x = 0.1$–0.3 at 1400 °C, while lower temperatures (1200–1300 °C) showed significantly higher density of 94–99% for higher Ca ($x = 0.3$) content. Powders 3, 5, and 8 are anomalies for which $x = 0.3$ caused a slight decrease in relative densities compared to those from $x = 0.2$. Powder 8 sintered at 1400 °C, for example, had a sintered density for $x = 0.2$ of 97%, while for $x = 0.3$, the density was 93%. This is likely due to the increased amount of Ca, and thus the increased amount of liquid that forms during sintering, leaving behind voids when the Ca is reabsorbed into the crystal structure on the A-site during cooling. Thus, pores form within the volume at the grain boundaries and decrease the density of the sintered product. Note that porosity is not necessarily a negative, such as SOFC cathodes, which require sufficient porosity for efficient operation. It is also important to note that pressureless sintering was used for all samples to evaluate the effect of Ca doping. Application of external pressure would increase the sintered density, should that be desired.

Electrical conductivity

Figure 6 shows the electrical conductivity for sintered $La_{1-x}Ca_x(B1,B2,B3)O_3$ materials. Data are shown in semi-log plots versus 10,000 divided by absolute temperature. Thus, temperature increases from right to left. It can be seen that all powders show increasing electrical conductivity with increasing temperature. All powders also demonstrate increasing electrical conductivity as the amount of Ca doped onto the A-site is increased, with the exceptions of Powders 5, 7, and 8, which had a higher conductivity for $x = 0.2$ (20, 17, and 28 S cm^{-1}, respectively) than for $x = 0.3$ (5, 9, and 24 S cm^{-1}, respectively). Some powders show a negative value for 300 K. This is because the conductivity was less than 1 S cm^{-1}; thus, the logarithm of conductivity is necessarily less than 1. Powder 4 (Fig. 6d) exhibits a nearly constant, low electrical conductivity below 700 K for $x = 0$ (< 1 S cm^{-1}) and below 600K for $x = 0.1$ (1 S cm^{-1}). The higher Ca-content samples lack this behavior. Powder 9 shows a nearly constant, high electrical conductivity for $x = 0.2$ and 0.3 (> 65 S cm^{-1}) over the entire temperature range. Table 3 shows the electrical conductivity for Powders 1–9 with the conductivity of the end-member materials for comparison. Powder 9 compares well with results for $La_{0.6}Ca_{0.4}FeO_{3-\delta}$ of 91 S cm^{-1} (Song et al. 2020), exceeding this conductivity for $x = 0.2$ and 0.3, indicating the benefit of B-site substitution, since lower Ca amounts yielded higher conductivity in this study.

Figure 7 shows Arrhenius plots of log σT vs 10,000 T^{-1} for $La_{1-x}Ca_x(B1,B2,B3)O_3$ materials. Applying a linear fit to these Arrhenius plots allows one to determine the activation energy for conductivity, by multiplying the slope with Boltzmann's constant, 8.617×10^{-5} eV K^{-1} (Kolisetty et al. 2017). Table 4 shows the activation energy for the powders under consideration.

Note that Powder 4, with $x = 0$ and $x = 0.1$, was nonlinear in the Arrhenius plots, as was Powder 3 for $x = 0.1$, so those activation energies were not determined. For most powders, increasing the amount of Ca doping on the A-site results in a decreasing activation energy. Powders 5 and 6 had their lowest activation energy for $x = 0.2$, though for these powders that increase for $x = 0.3$ was minor and likely within experimental error (see Table 4).

Conclusions

Perovskites may be modified both by the cations present in the B-site and by those present in the A-site. For lanthanum perovskites with equi-atomic substitution of

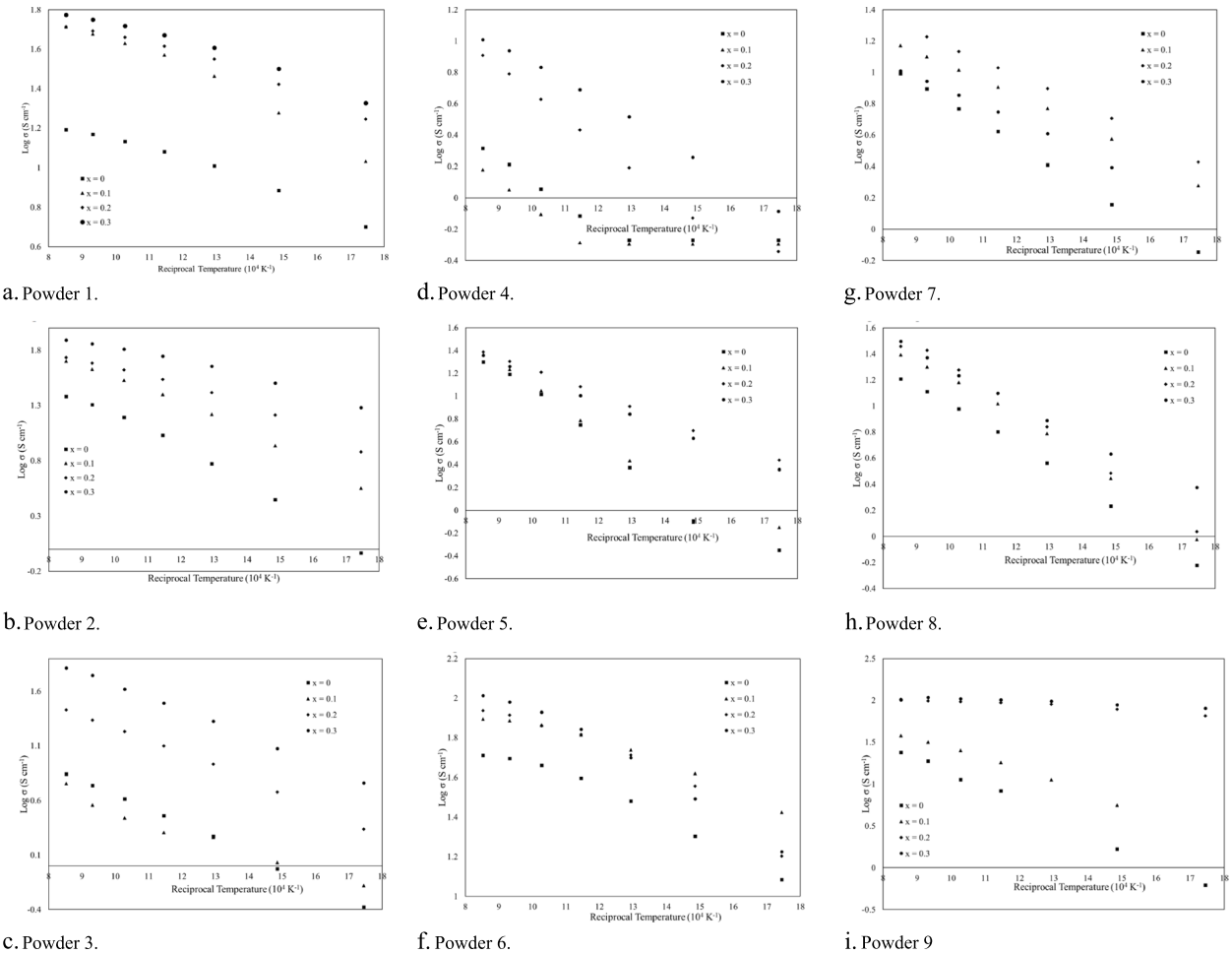

Fig. 6 Semi-log plots of electrical conductivity, σ, versus reciprocal temperature (10,000 K^{-1}) for $La_{1-x}Ca_x(B1,B2,B3)O_3$ materials. **a** Powder 1. **b** Powder 2. **c** Powder 3. **d** Powder 4. **e** Powder 5. **f** Powder 6. **g** Powder 7. **h** Powder 8. **i** Powder 9

Table 3 Electrical conductivity (S cm^{-1}) for sintered $La_{1-x}Ca_x(B1,B2,B3)O_3$ materials and $LaMO_3$ end-member compounds (where *M* = Co, Cr, Fe, Mn, and Ni) at 800 °C

Powder no. (B-site atoms)	$x = 0$	$x = 0.1$	$x = 0.2$	$x = 0.3$
1 (Cr, Fe, Ni)	14.71	47.60	49.25	56.18
2 (Cr, Co, Mn)	20.16	42.51	48.30	71.94
3 (Cr, Mn, Ni)	5.48	3.62	21.63	55.89
4 (Cr, Fe, Mn)	1.63	1.13	6.17	8.66
5 (Cr, Co, Fe)	15.53	17.16	20.15	18.25
6 (Cr, Co, Ni)	49.57	77.02	86.53	102.92
7 (Fe, Mn, Ni)	7.84	12.56	16.86	8.75
8 (Co, Fe, Mn)	12.86	19.97	26.81	23.56
9 (Co, Fe, Ni)	18.72	31.72	98.68	107.76
$LaCoO_3$ (Misusaki et al. 1989)	1000			
$LaCrO_3$ (700 °C) (Kharton et al. 1999)	0.34			
$LaFeO_3$ (Chiba et al. 1999)	0.1			
$LaMnO_3$ (He et al. 2008)	80			
$LaNiO_3$ (Chiba et al. 1999)	40			

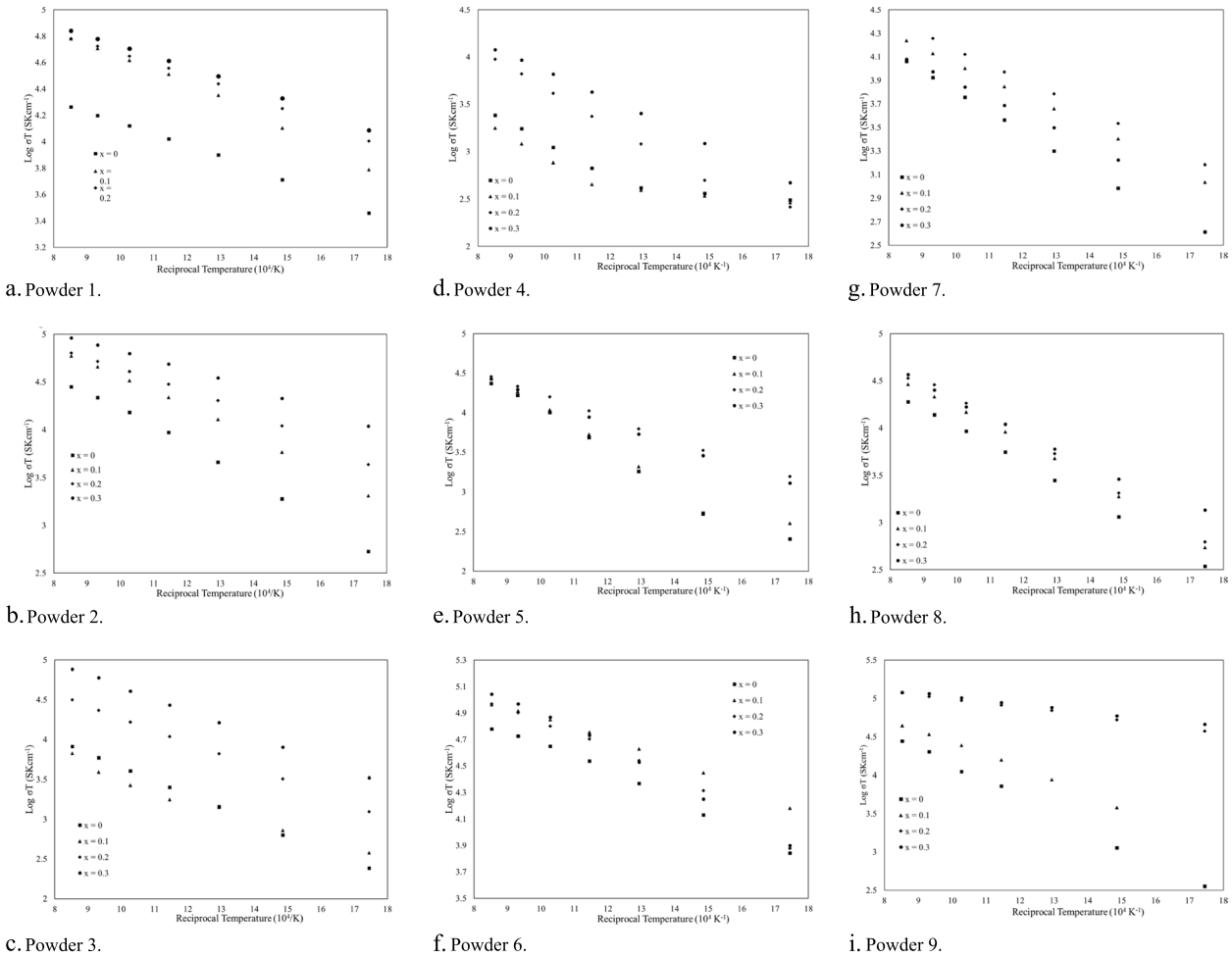

Fig. 7 Arrhenius plots of σT versus reciprocal temperature (10,000 K^{-1}) for sintered $La_{1-x}Ca_x(B1,B2,B3)O_3$ materials. **a** Powder 1. **b** Powder 2. **c** Powder 3. **d** Powder 4. **e** Powder 5. **f** Powder 6. **g** Powder 7. **h** Powder 8. **i** Powder 9

Table 4 Activation energy (eV) for sintered $La_{1-x}Ca_x(B1,B2,B3)O_3$ materials, from slopes of linear fits to data in Fig. 7

Powder no.	$x = 0$	$x = 0.1$	$x = 0.2$	$x = 0.3$
1	0.77	0.96	0.75	0.73
2	1.68	1.41	1.11	0.89
3	1.48	-	1.35	1.32
4	-	-	1.56	1.36
5	2.02	1.92	1.23	1.27
6	0.92	0.76	0.77	0.83
7	1.41	1.15	1.13	1.16
8	1.69	1.67	1.72	1.39
9	1.85	1.12	0.48	0.41

three B-site cations, doping with calcium on the A-site has multiple beneficial effects. First, Ca doping reduces the sintering temperature and increases the density for pressureless sintering in air. The formation of a liquid phase during sintering is the means by which the sintering behavior is improved. Second, increased calcium content increases the electrical conductivity from room temperature to 900 °C. Third, increasing calcium content decreases the activation energy for conductivity. Powder 9, $La_{0.7}Ca_{0.3}Co_{1/3}Fe_{1/3}Ni_{1/3}O_3$, had the lowest activation energy, 0.41 eV, with a conductivity of 108 S cm^{-1} at 800 °C. These results make it clear that one can tailor the properties of these perovskite materials by substitution on the B-site and doping on the A-site.

Acknowledgements
The authors would like to acknowledge the School of Mechanical, Aerospace, and Materials Engineering and the IMAGE facility at Southern Illinois University Carbondale for their valuable support during this research endeavor.

Authors' contributions
Dr. GAS wrote, drafted, and edited the manuscript. Dr. RK conceptualized the study. SRG coordinated, designed, carried out experiments, analyzed data, and wrote the "Electrical conductivity" section under "Results and discussion." All authors reviewed the manuscript.

Funding
Not applicable.

Availability of data and materials
The data and materials utilized in this study are available upon request from the corresponding author.

Declarations

Ethics approval and consent to participate
Not applicable.

Consent for publication
All authors have consented to the publication of this research paper.

Competing interests
The authors declare that they have no competing interests.

Received: 19 April 2024 Accepted: 17 June 2024
Published online: 22 June 2024

References

Chiba R, Yoshimura F, Sakurai Y (1999) An investigation of $LaNi_{1-x}Fe_xO_3$ as a cathode material for solid oxide fuel cells. Solid State Ionics 124:281–288
Gajjala SR, Fu Z, Koc R (2019) Investigation of (La_{1-X}, C_aX) $(N_{i0.2}5_{F0.2}5C_{r0.2}5C_{o0.2}5)_O3$ for solid oxide fuel cells cathode materials. Ceram Engr Sci Proc. 39–2:85–97
Gálvez ME, Jacot R, Scheffe J, Cooper T, Patzkeb G, Steinfeld A (2015) Physicochemical changes in Ca, Sr and Al-doped La–Mn–O perovskites upon thermochemical splitting of CO_2 via redox cycling. Phys Chem Chem Phys. 17:6629–6634
He Q, Zhang X, Hao H, Hu X (2008) High-temperature electronic transport properties of $La_{1-x}Ca_xMnO_{3+\delta}$ ($0.0 \leq x \leq 1.0$). Physica B 403:2867–2871
Kharton V, Yaremchenko A, Naumovich E (1999) Research on the electrochemistry of oxygen ion conductors in the former Soviet Union. II Perovskite-Related Oxides. J Solid State Electrochem. 3:303–326
Koc R, Anderson H (1992) Investigation of strontium-doped $La(Cr, Mn)_O3$ for solid oxide Fuel Cells. J Mater Sci. 27:5837–5843
Kolisetty A, Fu Z, Koc R (2017) Development of $La(CrCoFeNi)O_3$ system perovskites as interconnect and cathode materials for solid oxide fuel cells. Ceram Intl. 43:7647–7652
Liu J, Deng C, Liu X, Shao S, Zheng P, Chen L, Wu P, Li H, Ji H, Zhu W (2023) Single Mo atoms stabilized on high-entropy perovskite oxide: a frontier for aerobic oxidative desulfurization. Inorgan Chem 62(28):11044–11055
Misusaki J, Yoshiro M, Yamauchi S, Fueki K (1989) Electrical conductivity and Seebeck coefficient of nonstoichiometric $La_{1-x}Sr_xCoO_{3-\delta}$. J Electrochem Soc. 136:2082–2088
Pechini MP (1967) Method of preparing lead and alkaline earth titanates and niobates and coating method using the same to form a capacitor. US Patent 3(330):697
Sehlin S, Anderson H, Koc R, Sparlin D (1991) Evidence for 2+-4+ pairing in the (La, Ca)(Cr, Co_j)O3 series. Ceram Trans. 24:249–256
Song J, Ning D, Bouwmeester H (2020) Influence of alkaline-earth metal substitution on structure, electrical conductivity and oxygen transport properties of perovskite-type oxides $La_{0.6}A_{0.4}FeO_{3-\delta}$ (A = Ca, Sr and Ba). Phys Chem Chem Phys. 22:11984–11995
Sparlin D, Raffaelle R (1991) Theoretical and experimental implications of self compensation in the RMO_3 perovskite structure. Ceram Trans. 24:221–227

Publisher's Note